Physica E 120 (2020) 114074

Contents lists available at ScienceDirect

Physica E: Low-dimensional Systems and Nanostructures

journal homepage: www.elsevier.com/locate/physe

Magnetic properties of β_{12}-borophene in the presence of electric field and dilute charged impurity

Khang D. Pham [a,b], Nguyen D. Hien [c], Nguyen N. Hieu [d,*], Le T.T. Phuong [e,*]

[a] Laboratory of Applied Physics, Advanced Institute of Materials Science, Ton Duc Thang University, Ho Chi Minh City, Viet Nam
[b] Faculty of Applied Sciences, Ton Duc Thang University, Ho Chi Minh City, Viet Nam
[c] Nha Trang National Ethnic Minority Pre-university, Nha Trang City, Khanh Hoa Province, Viet Nam
[d] Institute of Research and Development, Duy Tan University, Da Nang, Viet Nam
[e] Center for Theoretical and Computational Physics, University of Education, Hue University, Hue City, Viet Nam

ABSTRACT

Monoatomic lattice of boron atoms (borophene), a new low-dimensional material shows promising physical and chemical properties. Recently, on the most stable borophene, metal β_{12}-borophene, electronic phase transition from metal-to-semimetal and metal-to-semiconductor in the presence of perpendicular electric field and dilute charged impurity is found, respectively. From this point, in this paper, we study the magnetic properties of the electric field and charged impurity induced β_{12}-borophene. Particularly, we have calculated Pauli spin paramagnetic susceptibility (PSPS) quantity using the five-band tight-binding Hamiltonian and the Green's function approach for different interaction-dependent models. The charged impurity and perpendicular electric field effects on the susceptibility of β_{12}-borophene show that the "pristine" PSPS of inversion symmetric model in β_{12}-borophene is larger than the homogeneous model as well as the Dirac fermions contribute to the total PSPS more than triplet fermions. Further, we found out that the dilute charged impurity does not influence PSPS of the principle system significantly at all temperatures and it decreases slightly with impurity concentration and scattering potential. On the other hand, electric field-induced PSPS results in an increasing (decreasing) trend for PSPS at very low (intermediate and high) temperatures. Our findings pave the way for the industrial practical applications.

1. Introduction

Following the successful synthesizing of the two-dimensional (2D) boron sheet, namely borophene, on an Ag substrate [1,2], many interests have been drawn to group III elements [3–7]. Elemental boron has placed at the boundary between metals and non-metals in the periodic table possessing rich chemistry. The electron shell configuration of boron with three valence electrons and its flexibility to adopt different hybridizations lead to forming complex B-B bondings ranging from two-center-two electron to seven-center-two electron bonds, therefore, various boron allotropes exist in all-dimensions [8–12]. Unlike bulk boron systems that behave as a semiconductor, 2D structures of boron which have been experimentally synthesized including striped, β_{12}, χ_3, and honeycomb phases have metallic phase. Borophene illustrates special physical properties, for instance, investigation of the mechanical properties of striped borophene with buckling height of 0.91 Å shows highly anisotropic feature, so that the value of critical strains are 8% and 15% along the a-direction and b-direction, respectively [13]. Also, the extraordinary features of borophene such as high mechanical anisotropy properties [1], novel magnetism and electronic phase transition [14] make it a promising candidate for the future design of nano-electronic devices [15,16].

Recently, many theoretical calculations are done aiming at the study of borophene physical properties including electronic, optical, lattice thermal conductivity, mechanical, superconducting and phonon dispersion properties, since synthesizing borophene under the strict experimental conditions has carried out slowly and difficulty [13,17–21]. On the basis of density functional theory (DFT) analysis, L. Adamska et al. [22] pointed out that the optical absorbance and electronic band structure of β_{12} and δ_6 can be tuned in the presence of few percents of strain. Also, the authors have reported that applying strains up to 6% can modify band structure, the in-plane anisotropy of the complex dielectric function and eventually the optical absorption of both the above-mentioned structures without any electronic phase transition. On the other hand, Zhang et al. [23] have predicted the great potential of two β_{12} and χ_3 phases of borophene for Li-ion and Na-ion batteries technologies with extremely high power density. Also, B. peng et al. [24] has investigated the electronic, optical, and thermodynamic features of striped borophene using DFT calculations, exhibiting striped borophene possesses high optical transparency and electrical conductivity, which increase its applications in photovoltaics and flexible electronics industry.

Here we focus on β_{12}-borophene phase which is the most stable geometry thermodynamically, mechanically and dynamically [25]. In

* Corresponding authors.
E-mail addresses: phamdinhkhang@tdtu.edu.vn (K.D. Pham), hieunn@duytan.edu.vn (N.N. Hieu), lttphuong@hueuni.edu.vn (L.T.T. Phuong).

https://doi.org/10.1016/j.physe.2020.114074
Received 31 January 2020; Received in revised form 27 February 2020; Accepted 4 March 2020
Available online 7 March 2020

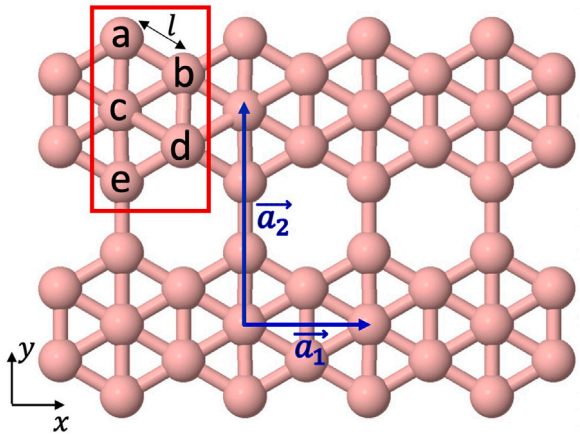

Fig. 1. Top view of the atomic structure of β_{12}-borophene sheet. The red rectangle shows the unit cell of β_{12}-borophene with five boron atoms. The lattice basis vectors are given by $\vec{a}_1$ and $\vec{a}_2$. (For interpretation of the references to color in this figure legend, the reader is referred to the web version of this article.)

the work by Le et al. [26], it is reported that the electric phase of β_{12}-borophene can be tuned via electric field and charged impurity, so that charged impurity induced β_{12}-borophene behaves as a semimetal at high scattering potentials as well as applying electric field opens a band gap in β_{12}-borophene and it behaves like a semiconductor. In the present work, with the purpose of exploring novel magnetic properties of β_{12}-borophene, we seek to theoretically deal with the magnetic properties of the perpendicular electric field- and impurity-infected β_{12}-borophene corresponding to semiconductor and semimetal phase, respectively. To do so, we use the tight-binding Hamiltonian model, the Green's function approach and the Born approximation in our numerical calculations.

The setup of the paper is as follows. Section 2 describes the geometric structure and tight-binding Hamiltonian of β_{12}-borophene as well as the electronic band structure of all considered models. Also, the formulation of magnetic susceptibility using the electronic density of states (DOS) is presented. The perturbed Green's function of β_{12}-borophene in the presence of dilute charged impurity as well as the corresponding results for the magnetic susceptibility of impurity-infected β_{12}-borophene are investigated in Section 3. The biased Hamiltonian and magnetic susceptibility of β_{12}-borophene is brought in Section 4. Finally, Section 5 concludes.

2. Theoretical formulation

2.1. Hamiltonian model for pristine β_{12}-borophene

It is useful to understand the lattice structure and hybridization of atomic orbitals in β_{12}-borophene, before going to its tight-binding details. Fig. 1 presents the atomic structure and the unit cell of β_{12}-borophene. As can be seen from the figure, the red rectangle shows the unit cell of β_{12}-borophene, consisting of five boron atoms including a, b, c, d, and e atoms which are located at different sites in the unit cell. Different bonds of boron atoms lead to different on-site potentials for boron atoms in the unit cell. Also, $\vec{a}_1$ and $\vec{a}_2$ are the lattice basis vectors given by $\vec{a}_1 = \sqrt{3}l\hat{e}_x$ and $\vec{a}_2 = 3l\hat{e}_y$, where $l \simeq 1.69$ Å denotes the distance between B-B atom. According to findings in Ref. [23], the values of lattice parameters of the β_{12}-borophene are 2.926 Å and 5.068 Å for $|\vec{a}_1|$ and $|\vec{a}_2|$, respectively. Also, the first Brillouin zone (FBZ) of β_{12}-borophene is a rectangle which is characterized by the lattice parameters $-\pi/a_1 \leq k_x \leq \pi/a_1$, and $-\pi/a_2 \leq k_y \leq \pi/a_2$ along the x and y directions, respectively [27]. Using a convention shift, the area of Brillouin zone along x direction can be rewritten as $0 \leq k_x \leq 2\pi/a_1$.

From the lattice of β_{12}-borophene, two mirror symmetries M_x and M_y with respect to the x and y axes, respectively, are present and because of these two, an inversion symmetry operator $I = M_x M_y$ appears with respect to the center of the honeycomb, i.e. c atom.

It is well known that the p_z orbitals form π bands near the Fermi level and the Dirac cones locate at K points in graphene [24,28–30]. Similar to graphene, the β_{12}-borophene sheet also has an atomically flat structure and the s, p_x, and p_y orbitals make a sp^2 hybridization contributing to the σ bands which are far from the Fermi level, thus, the bands near the Fermi level are owing to the p_z orbital of the boron atoms corresponding to π bonds, in agreement with recent experiments and first-principles calculations [31,32]. From this point, we formulate the effective Hamiltonian of β_{12}-borophene only in terms of the p_z orbital in the real space as

$$\hat{\mathcal{H}}^{(0)} = \sum_i \varepsilon_i \hat{f}_i^\dagger \hat{f}_i + \sum_{i,j} t_{ij} \hat{f}_i^\dagger \hat{f}_j + \text{H.c.}\,, \tag{1}$$

where $\hat{f}$ can be each of the $\{\hat{a}, \hat{b}, \hat{c}, \hat{d}, \text{or } \hat{e}\}$ atoms in the unit cell. Also, ε_i refers to the on-site energy for electrons at the ith site of the lattice. The coefficient t_{ij} is the hopping parameter between nearest-neighbor atomic sites i and j. The Hamiltonian in the real space can be easily transferred to the momentum space using the Fourier transformation in which the annihilation and creation operators read as

$$\hat{f}_i = \frac{1}{\sqrt{N_a}} \sum_{\vec{k}} e^{-i\vec{k}.\vec{r}_i} \hat{f}_{\vec{k}} \quad , \quad \hat{f}_i^\dagger = \frac{1}{\sqrt{N_a}} \sum_{\vec{k}} e^{+i\vec{k}.\vec{r}_i} \hat{f}_{\vec{k}}^\dagger\,, \tag{2}$$

where N_a and $\vec{\mathrm{r}}_i$ are the number of atoms and the position vector of ith unit cell, respectively. Then the Hamiltonian can be expressed in the matrix form of

$$\hat{\mathcal{H}}_{\vec{k}} = \begin{pmatrix} \mathcal{H}_{aa} & \mathcal{H}_{ab} & \mathcal{H}_{ac} & \mathcal{H}_{ad} & \mathcal{H}_{ae} \\ \mathcal{H}_{ba} & \mathcal{H}_{bb} & \mathcal{H}_{bc} & \mathcal{H}_{bd} & \mathcal{H}_{be} \\ \mathcal{H}_{ca} & \mathcal{H}_{cb} & \mathcal{H}_{cc} & \mathcal{H}_{cd} & \mathcal{H}_{ce} \\ \mathcal{H}_{da} & \mathcal{H}_{db} & \mathcal{H}_{dc} & \mathcal{H}_{dd} & \mathcal{H}_{de} \\ \mathcal{H}_{ea} & \mathcal{H}_{eb} & \mathcal{H}_{ec} & \mathcal{H}_{ed} & \mathcal{H}_{ee} \end{pmatrix}. \tag{3}$$

The elements of these matrices are described as follows:

$$\begin{aligned} \mathcal{H}_{aa} &= \frac{1}{N} \sum_{n'=1}^{N} \sum_{n=1}^{5} \int d\mathbf{r} e^{-i\vec{k}.(\mathbf{R}_n^a - \mathbf{R}_{n'}^a)} \\ &\times \left[\phi_{\vec{k}}^*(\mathbf{r} - \mathbf{R}_{n'}^a) \mathcal{H}_{\vec{k}} \phi_{\vec{k}}(\mathbf{r} - \mathbf{R}_n^a)\right] \\ &\approx \begin{cases} 0, & n \neq n' \\ \varepsilon_a, & n = n' \end{cases}. \end{aligned} \tag{4}$$

The integral in Eq. (4) only survives for $n = n'$, otherwise, it is zero, which means that there is no hopping between electrons of the same atoms in different unit cells. In a similar way, the same results hold for the elements $\mathcal{H}_{bb}, \mathcal{H}_{cc}, \mathcal{H}_{dd}$, and $\mathcal{H}_{ee}$. The major interaction between nearest neighbors is obtained by the off-diagonal elements $\mathcal{H}_{ij}$. The element $\mathcal{H}_{ab}$ is calculated as

$$\mathcal{H}_{ab} \approx t_{ab} g_{\vec{k}} \quad , \quad \mathcal{H}_{ac} \approx t_{ac} f_{\vec{k}}\,. \tag{5}$$

In $\mathcal{H}_{ab}$ relation, the summations indices n and n' shown in Eq. (4) run over the all a and b sublattices in the crystal, respectively. One can carry out the summation over all the atoms in the crystal ($n' = 1, 2, .., N$) and at each step it sums over the five nearest neighbor atoms b ($n = 1, 2, 3, 4, 5$) by considering only the effects of nearest-neighbor interaction. By repeating these calculations $\mathcal{H}_{ba}$ and $\mathcal{H}_{ca}$ can be obtained as

$$\mathcal{H}_{ba} = \mathcal{H}_{ab}^* = t_{ab} g_{\vec{k}}^* \quad , \quad \mathcal{H}_{ca} = \mathcal{H}_{ac}^* = t_{ac} f_{\vec{k}}^*\,. \tag{6}$$

The $f_{\vec{k}}$ and $g_{\vec{k}}$ are the geometrical factors which both are obtained as

$$g_{\vec{k}} = 2e^{ia_1 k_y/2\sqrt{3}} cos(a_1 k_x/2) \quad , \quad f_{\vec{k}} = e^{ia_1 k_y/2\sqrt{3}}\,. \tag{7}$$

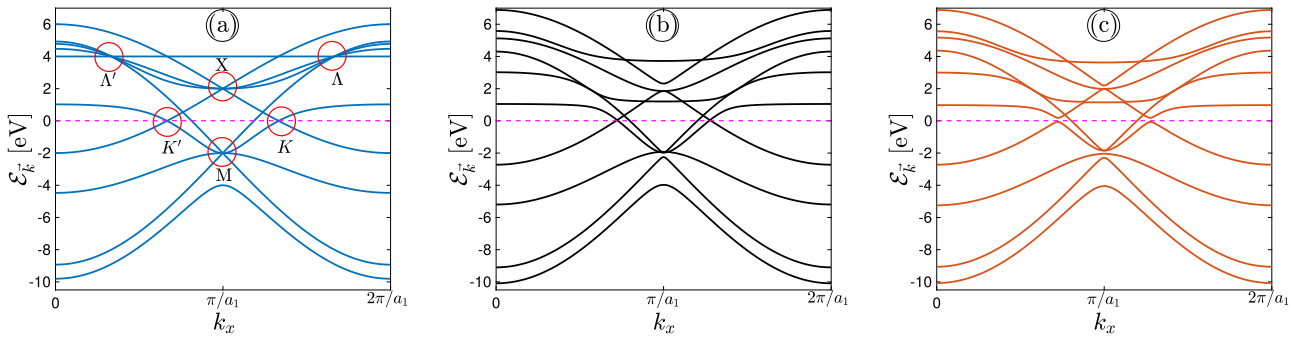

Fig. 2. (Color online) Electronic band structure of β_{12}-borophene for (a) homogeneous, (b) inversion symmetric and (c) inversion nonsymmetric model. K, K' show two Dirac fermions, X and M correspond to the triplet fermions and Λ and Λ' form three-band crossing points.

Furthermore, other off-diagonal elements can be obtained in the same way. Consequently, we obtain

$$\hat{\mathcal{H}}_{\vec{k}} = \begin{pmatrix} \varepsilon_a & t_{ab}g_{\vec{k}} & t_{ac}f^*_{\vec{k}} & 0 & t_{ae}f_{\vec{k}} \\ t_{ab}g^*_{\vec{k}} & \varepsilon_b & t_{bc}g_{\vec{k}} & t_{bd}f^*_{\vec{k}} & 0 \\ t_{ac}f_{\vec{k}} & t_{bc}g^*_{\vec{k}} & \varepsilon_c & t_{cd}g_{\vec{k}} & t_{ce}f^*_{\vec{k}} \\ 0 & t_{bd}f_{\vec{k}} & t_c g^*_{\vec{k}} & \varepsilon_d & t_{de}g_{\vec{k}} \\ t_{ae}f^*_{\vec{k}} & 0 & t_{ce}f_{\vec{k}} & t_{de}g^*_{\vec{k}} & \varepsilon_e \end{pmatrix}, \tag{8}$$

Table 1 shows the values of the hopping parameter obtained from DFT knowledge [31]. Actually, an effective Dirac theory for general parameters are derived in Ref. [27] to confirm the first-principle calculations of the Ref. [31]. Depending on the interaction between boron atoms and Ag atoms in the sublayer, there are three models for β_{12}-borophene including homogeneous model, inversion nonsymmetric model, and inversion symmetric model. In the homogeneous model, all hopping parameters set to −2 eV as well as the on-site potentials are equal to zero. In inversion symmetric model, the on-site energies are given by

$$\varepsilon_a = \varepsilon_d = 0.196 \text{ eV}, \varepsilon_b = \varepsilon_e = 0.058 \text{ eV}, \varepsilon_c = 0.845 \text{ eV}. \tag{9}$$

In the case of inversion nonsymmetric model, Ag atoms effects lead to inversion symmetry breaking of the lattice structure, thus, the values of on-site potentials are given by

$$\varepsilon_a = \varepsilon_e = 0.196 \text{ eV}, \varepsilon_b = \varepsilon_d = 0.058 \text{ eV}, \varepsilon_c = 0.845 \text{ eV}. \tag{10}$$

When the β_{12}-borophene is placed on a Ag(111) substrate, it has been shown that a long-range modulation, yielding an electronic perturbation, arising from the lattice mismatch gives rise to a moiré pattern [31], simulating by varying the on-site energy over a superlattice period in their tight-binding model. By this, the Dirac fermions become gapped in the inversion nonsymmetric model, implying that the inversion symmetry breaking occurs.

Now, by diagonalizing the Hamiltonian in Eq. (8), we can numerically obtain the electronic band structure of β_{12}-borophene for all three models, as shown in Fig. 2. The Fermi level is set to zero. From the figure, we can see that the conduction and valence bands touch each other at the Fermi energy, as a result of this, all three models have a metallic phase. Also, six high-symmetry points which play key roles in our numerical calculations, are shown in the band structure diagram of homogeneous model: $K(2\pi/3a_1, 0), K'(-2\pi/3_1, 0)$ as two Dirac fermions, $X(\pi/a_1, 0)$ and $M(\pi/a_1, -\pi/a_2)$ corresponding to the triplet fermions, and $\Lambda(\pi/3a_1, \pi/a_2)$ and $\Lambda'(-\pi/3a_1, \pi/a_2)$ that form three-band crossing points. We would like to comment why we get 10 bands in the band structures. From the coordinates of six high-symmetry points, it is clear that the value of k_y is zero for K, K' and X points, while M, Λ and Λ' are appeared in $k_y = \pi/a_2$. Therefore, in order to have all six high-symmetry points in a 2D band structure, we have plotted the band structure of β_{12}-borophene as a function of k_x for these two k_ys and for each of them we have 5 bands, as a results of this, we have 10 bands in general. At a closer glance, it can be found that removing the c atoms from the structure of the β_{12}-borophene makes a honeycomb structure like graphene. Therefore, it is expected to β_{12}-borophene possesses massless Dirac fermions, however, in Fig. 2(c) massive Dirac points are observed for inversion nonsymmetric model. For this reason, we will only focus on the results of the homogeneous and inversion symmetric models in which the massless Dirac fermions are taking a role in the metallic phase of the lattice.

Table 1
Hopping energies for inversion symmetric and inversion nonsymmetric models.
Source: Taken from Ref [31].

Hopping energy	Value [eV]	Hopping energy	Value [eV]
$t_{ab} = t_{de}$	−2.04	$t_{ac} = t_{ce}$	−1.79
t_{ae}	−2.12	$t_{bc} = t_{cd}$	−1.84
t_{bd}	−1.91		

2.2. Pauli spin paramagnetic susceptibility

It is a known fact that magnetic materials show an internal magnetization ($\mathcal{M}$) under an external magnetic field (H), as a perturbation, as well as magnetic susceptibility χ is the ratio of this induced magnetization to the applied magnetic field strength. Depending on the behavior of materials under the external magnetic field, these divided into three main groups including antiferromagnetic (AFM), paramagnetic (PM) and ferromagnetic (FM).

Pauli spin paramagnetic susceptibility is a valid model for most paramagnetic metals with free electrons. In this model, it is supposed that the conduction electrons should be free as well as applying the external magnetic field creates an imbalance between electrons with an opposite spin which leads to a low magnetization in the same direction as the applied field. PSPS of a material χ, can be calculated in terms of DOS using $D(\mathcal{E}) = -(1/\pi N_a)\sum_{\vec{k}\in FBZ}\sum_{\alpha=1}^{5} \text{Im}\, G_{\alpha\alpha}(\vec{k}, \mathcal{E})$ [$N_a = 5$ is the number of atoms per unit cell, see Appendix A for more details]. First of all, the magnetization density reads [33–36]

$$\mathcal{M} = \frac{\mu_B}{2}\int_{-\infty}^{\infty} D(\mathcal{E})d\mathcal{E}\left[f(\mathcal{E} - \mu_B H) - f(\mathcal{E} + \mu_B H)\right], \tag{11}$$

where the Fermi–Dirac distribution function is given by $f(\mathcal{E}, T) = 1/[e^{\mathcal{E}/k_B T} + 1]$. k_B is the Boltzmann constant and μ_B is the Bohr magneton. Then, we have [see Appendix B for more details]

$$\mathcal{M} = \mu_B^2 H \int_{-\infty}^{\infty} D(\mathcal{E})\frac{-\partial f(\mathcal{E}, T)}{\partial \mathcal{E}} d\mathcal{E}, \tag{12}$$

in which the PSPS can be written as

$$\chi(T) = \mu_B^2 \int_{-\infty}^{\infty} D(\mathcal{E})[-\partial_{\mathcal{E}} f(\mathcal{E}, T)]d\mathcal{E}. \tag{13}$$

Evidently, the PSPS of the clean and perturbed system can be computed by replacing clean or perturbed $D(\mathcal{E})$. This quantity is eminently

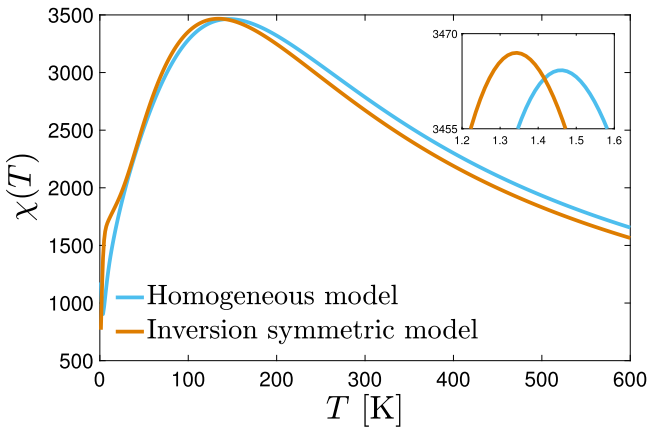

Fig. 3. (Color online) PSPS of homogeneous and inversion symmetric models of β_{12}-borophene as a function of absolute temperature.

suitable to classify solid materials based on their magnetic properties. In the following, we deal with the PSPS of electric field and charged impurity induced β_{12}-borophene.

It is appropriate to remind a brief review of magnetic materials. In FM materials, the dipole moments of atoms or ions strongly coupled to each other separately with parallel magnetization. Not only under an applied magnetic field, but also in the absence of magnetic field, atoms or ions in FM materials affect on each other and try to parallel their magnetic moments because of the exchange coupling forces between the spin of different atoms and ions. Also, there is a critical temperature so-called Curie temperature T_C above which the permanent magnetic properties have vanished. In addition, PM is a weakly form of magnetic properties of the material. In these material atoms or ions have separately permanent magnetic moments and in the presence of an external magnetic field, an internal magnetic fields form in the direction of the applied magnetic field. In AFM material, there are two or more sublattices that are magnetized in opposite directions. Similar to FM materials AFM materials become PM above a critical temperature namely Neel temperature T_N which is obtained from the peak of the susceptibility. The value of PSPS is maximum at $T = T_N$ and reduces by increasing in T. It should be noted that we set values of physical constants μ_B and k_B to unity in order to simplify the numerical calculations. Let us focus on the pristine results of PSPS in β_{12}-borophene.

Fig. 3 presents the pristine PSPS curve of β_{12}-borophene for both homogeneous and inversion symmetric models as a function of temperature. From the figure, we can see the PSPS curves for both mentioned models first increase and then after reaching a maximum value decrease, therefore, these models have the AFM phase. Also, on the basis of DFT calculations, in Ref. [14], the authors have addressed the magnetic properties of striped borophene nanoribbons, finding the anisotropic quasi-planar geometric structure of striped borophene nanoribbon. Further, it has been found that the edge states are largely govern to its electronic and magnetic properties, so that striped borophene nanoribbons are non-magnetic along x-direction, while they behave as an AFM or FM depending on the ribbon width along y-direction, which is almost in agreement with our results. However, the value of T_N is not the same for both models and the inversion symmetric model has a little less T_N in comparison with the homogeneous model. Besides, as highlighted in the inset panel, we can find that the height of χ in the inversion symmetric model is more than one in the homogeneous model. The physical reason behind it is the existence of a direct relation between DOS and PSPS [see Eq. (13)]. Also, according to the band structure dispersion diagrams, which are shown in Fig. 1, the concavity of bands in the inversion symmetric model is more than homogeneous one, as a result of this the inversion symmetric model has

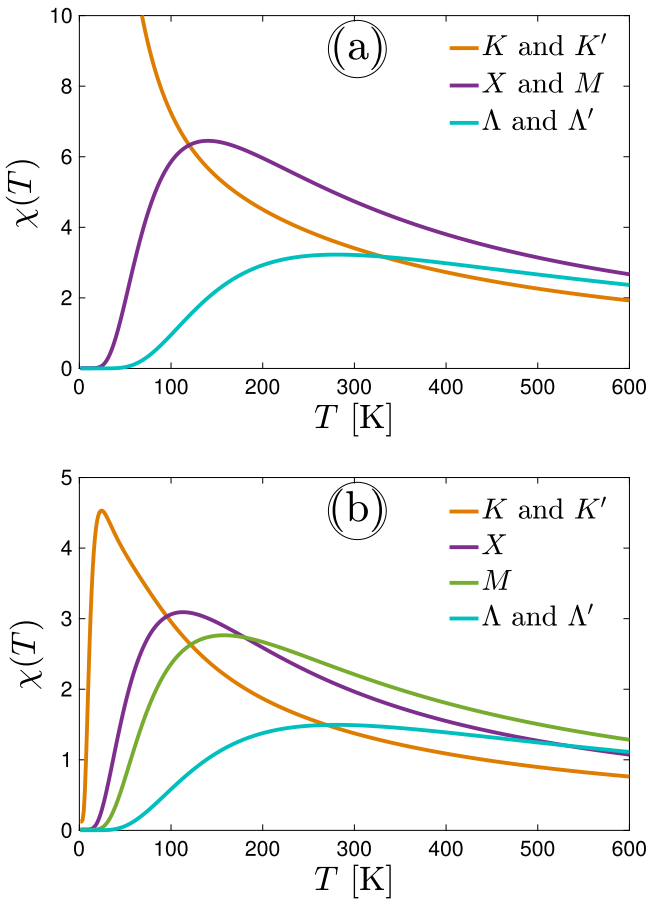

Fig. 4. (Color online) Susceptibility of high-symmetry points in the FBZ of β_{12}-borophene for (a) homogeneous and (b) inversion symmetric model when the thermal energy induced to the system is increased.

more degenerated states than homogeneous model leading to higher value for DOS and eventually higher PSPS. This, in turn, means that the interaction between the boron atoms and the substrate atoms in homogeneous model is stronger than the inversion symmetric model because the system is less sensitive to the external magnetic field and the spins in the case of homogeneous model are not interested as much as the inversion symmetric one in responding to the magnetic field.

As mentioned before, the total metallic electronic phase of β_{12}-borophene stems from the low-energy Dirac points, i.e. K and K' points. By this, a higher PSPS is expected in the χ plots independent of the model, as confirmed in Fig. 4. Particularly, the contribution of different momenta in the total PSPS of the system is studied in the following to see what the contribution order of high symmetry points in the FBZ is in the entire response of the lattice to the external magnetic field. In other words, the interband transition contributions to the total response of the system are clarified, which helps to figure out how the electronic phase of the system can be influenced by the magnetic doping. As explained before as well as addressed in the work of Ezawa [27], the inversion symmetric model is the best model close to the experiment. Thus, the AFM phase of the system should be seen in the inversion symmetric model, not in the homogeneous one. Shortly, we would stress that the results are in a good agreement with the graphene ones, as expected.

Fig. 4 illustrates the PSPS of the high symmetry points in the FBZ of β_{12}-borophene including K, K', X, M, Λ, and Λ' points for the (a) homogeneous and (b) inversion symmetric model. Fig. 4(a) confirms clearly the expected non-AFM phase of the system when the homogeneous model is responsible for the dynamics of carriers, whereas Fig. 4(b)

shows that the K and K' points mostly contribute to the total AFM phase of the system, in agreement with expectations above-explained. It is clear that the PSPS of K and K' as well as Λ and Λ' show the same behaviors, for both models, while the PSPS of the X and M points behave similarly to each other only in the homogeneous model. Also, in panel (a) we observe that the susceptibility of K and K' behaves as a PM, whereas the PSPS of these points exhibits AFM phase in inversion symmetric model. In addition, the PSPS of Λ and Λ' points shows AFM phase for both models, but with differences that the height of χ in the homogeneous model (a) is more than inversion symmetric model (b) as well as the T_N shifts to lower values in (b) model in comparison with (a). In the case of PSPS of X and M points, we can see that they behave as an AFM but they do not show exactly similar behaviors because as illustrated in Fig. 2(b) they do not have same electronic band dispersion and two bands cross each other at X point whereas triplet fermions emerge at M point. Thereby, the Dirac fermions and triplet fermions do not contribute similarly to the total system dynamics. Such behaviors are also seen in other 2D materials [37,38].

As mentioned before, charged impurity induced β_{12}-borophene behaves as a semimetal as well as the electric phase of β_{12}-borophene changes from metal to semiconductor when an electric field is applied [26]. For this reason, in the following, we will study the PSPS of metal, semimetal and semiconductor β_{12}-borophene for two homogeneous and inversion symmetric models in the presence of dilute charged impurity (Section 3) and electric field (Section 4).

3. Impurity infected β_{12}-borophene

In this section, we address the effects of charged dilute impurity with different concentrations n_i and scattering potential v_i on the PSPS of β_{12}-borophene. It is worthwhile noting that, substituting Hamiltonian of β_{12}-borophene in the below equation gives us the clean Green's function of correlated electronic waves or orbitals in the system

$$\hat{G}^{(0)}(\vec{k},\mathcal{E}) = \left[(\mathcal{E}+\mathrm{i}\eta)\hat{\mathbf{I}} - \hat{\mathcal{H}}_{\vec{k}}\right]^{-1}. \tag{14}$$

where $\eta = 5$ meV is the broadening factor of correlated electronic waves. Moreover, summing over the imaginary part of the Green's function matrix reaches the *clean* DOS of β_{12}-borophene

$$D^{(0)}(\mathcal{E}) = \frac{-1}{\pi N_a}\sum_{\vec{k}\in FBZ}\sum_{\alpha=1}^{5}\mathrm{Im}\,G^{(0)}_{\alpha\alpha}(\vec{k},\mathcal{E}). \tag{15}$$

where α implies the sublattices.

Aiming at the investigation of the dilute charged impurity and its impacts on the magnetic properties of β_{12}-borophene, we formulate the perturbed DOS of the system using the Born approximation in the scattering theory and T-matrix [39]. The impurities are doped *randomly* to the system and just the values of their concentration and scattering potential play role in our computations. In the Born approximation, the electron–impurity interaction can be included in the self-energy, $\Sigma(\mathbf{p},\mathcal{E})$, which is calculated as

$$\hat{\Sigma}(\mathbf{p},\mathcal{E}) = n_i v_i\left[1 - \frac{v_i}{N_a}\sum_{\vec{k}\in FBZ}\hat{G}^{(0)}(\vec{k},\mathcal{E})\right]^{-1}, \tag{16}$$

where $\mathbf{p}$ is the quantum wave-vector induced from the impurities to the Dirac and triplet fermions of β_{12}-borophene. However, for the isotropic scattering effects like what we have in our system, this self-energy depends only on the energy, not momenta. From this point, the perturbed Green's function can be obtained through the Dyson equation [39]

$$\hat{G}(\vec{k},\mathcal{E}) = \hat{G}^{(0)}(\vec{k},\mathcal{E})\left[1 - \hat{G}^{(0)}(\vec{k},\mathcal{E})\hat{\Sigma}(\mathcal{E})\right]^{-1} \tag{17}$$

By this, simply, the electronic perturbed DOS is calculated using interacting Green's function matrix:

$$D(\mathcal{E}) = \frac{-1}{\pi N_a}\sum_{\vec{k}\in FBZ}\sum_{\alpha=1}^{5}\mathrm{Im}\,G_{\alpha\alpha}(\vec{k},\mathcal{E}). \tag{18}$$

leading to the impurity scattering effects on the electronic features of β_{12}-borophene.

Before anything, it would be nice to clarify some numerical notes, which are necessary to be polished. In our numerical calculations we have $n_i = N_i/N_{uc}$, in which N_i, N_{uc} refer to the number of impurity atoms and unit cells, respectively. Besides, we have performed the numerical calculations for 1000×1000 unit cells to obey the validity limit of T-matrix approximation for dilute regimes. Therefore, $n_i = 20\%$ means that 20% of all unit cells considered above is infected by impurity atoms only, for this reason, we would call it a dilute impurity compared to such a huge unit cell.

The temperature-dependent curves of the PSPS of β_{12}-borophene for both homogeneous (a, c) and inversion symmetric (b, d) models in the absence and presence of dilute charged impurity are exhibited in Fig. 5. Panel (a) and (b) are drawn under the condition that the value of scattering potential is set to 0.1 eV while the impurity concentration increases. Also, in panels (c) and (d), the impurity concentration is fixed at 10% for different scattering potentials. From these panels, it can be understood that the AFM phase of β_{12}-borophene for both homogeneous and inversion symmetric models remains constant even in the presence of dilute charged impurity. This means that the dilute regime does not work well for changing the magnetic phase of the principle system and the distribution of electronic orbitals is robust in the presence of such dilute perturbations. However, the inset panels show that an increase in the impurity concentration or scattering potential leads to a slow change in the height of χ and T_N. From panels (a) and (b) we can see that the maximum value of χ reduces by increasing in the n_i as well as the T_N already do not change in the homogeneous model, while in the case of inversion symmetric one it moves to higher temperatures when impurity concentration is equal to 5%. Furthermore, as shown in panels (c) and (d) any significant change is observed in the Neel temperature by increasing the scattering potential of charged impurities.

In a nutshell, there is no significant alteration in the response function of the system when it is subjected to the dilute charged impurities and the inset panels for fairly low and intermediate thermal energies report that there is no order for the trends when the impurity concentration or scattering potentials is increased similar to the graphene and most of the other 2D materials.

4. Biased β_{12}-borophene

Let us consider another perturbation, which changes the electronic phase of the system significantly [26], i.e. the electric field. Applying bias voltage is one of the common methods for tuning the band gap of 2D materials [40–42]. In Ref. [26], it is found that β_{12}-borophene suffers from a metal-to-p-doped semiconductor phase transition under a strong enough perpendicular electric field. Therefore, it is expected that magnetic properties of β_{12}-borophene show novel and interesting features in the presence of perpendicular electric field as well. One can apply the perpendicular electric field on the β_{12}-borophene by installing gate voltage on the top and bottom of its sheet. Thus, the tight-binding Hamiltonian of biased β_{12}-borophene in the real space can be written as

$$\hat{\mathcal{H}}^{\mathrm{EF}} = \hat{\mathcal{H}}^{(0)} + \frac{1}{2}\sum_i V_i \hat{f}_i^{\dagger}\hat{f}_i\,, \tag{19}$$

wherein V_i refers to the applied bias voltage. In this formalism, we do not consider the electric field effects on the c atom in the center of honeycomb lattices because of the electronic wave functions cancellation originating from the isotropic structure of our principle system. Lattice symmetries lead to the striped charging effects because in the case of β_{12}-borophene, there is a phase cancellation at the six-fold coordinated boron atom which leads to a vanishing amplitude at site c [31]. For this reason, the on-site potential for atom c is set to zero. Therefore, the atoms at sites a, b, d and e are the origin of the total wave-function and can be decomposed into two sublattices, first sublattice is made of

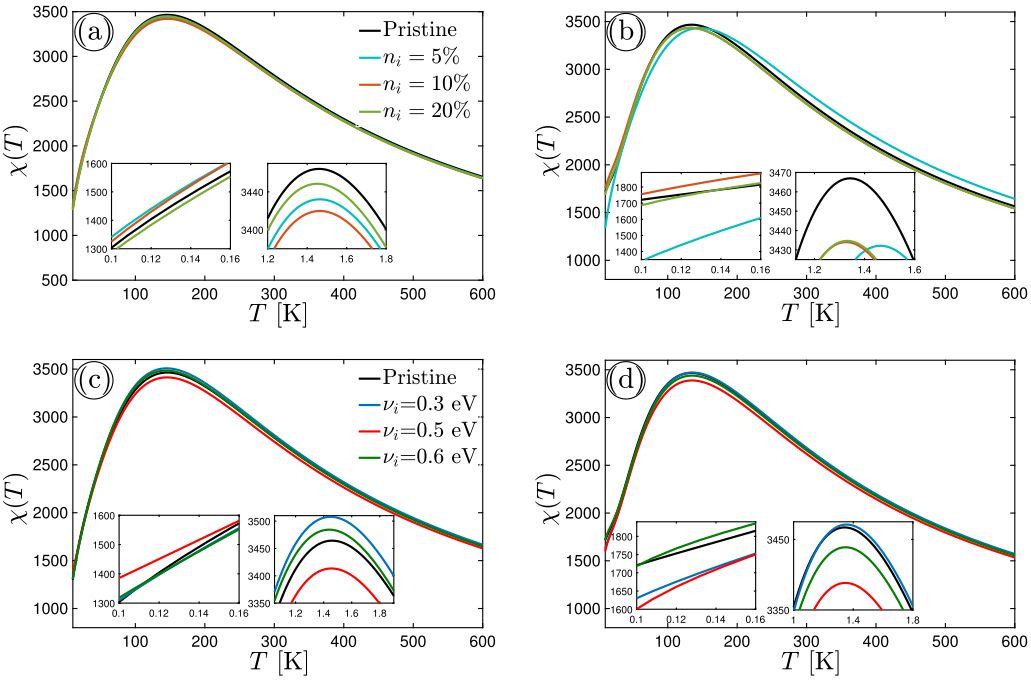

Fig. 5. (Color online) The magnetic susceptibility of dilute charged impurity infected β_{12}-borophene for (a, c) homogeneous and (b, d) inversion symmetric models. Panels (a, b) are drawn for different impurity concentrations, while the scattering potential is fixed at $\nu_i = 0.1$ eV, as well as, the fixed impurity concentration equal to 10% and different scattering potentials are considered for panels (c, d).

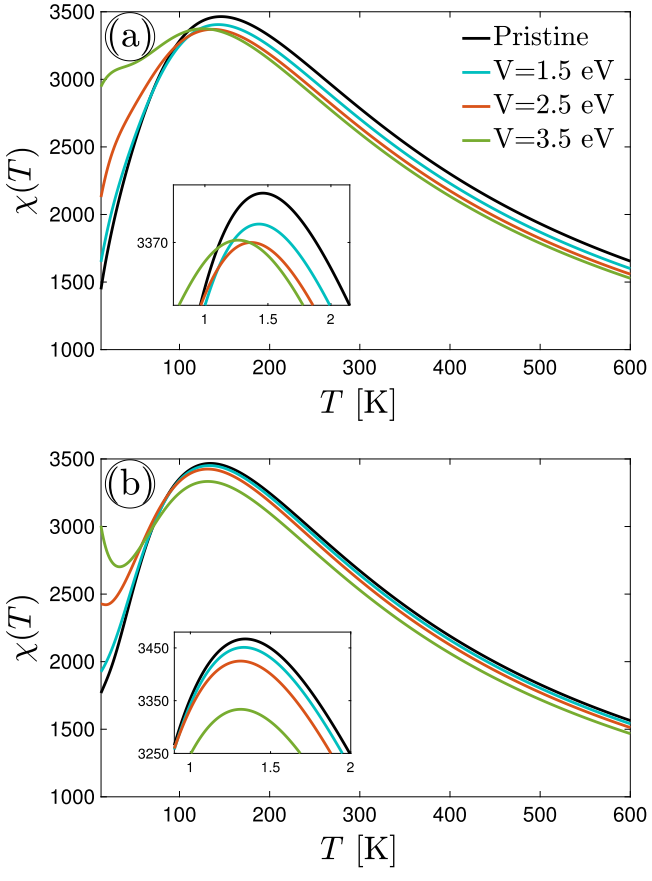

Fig. 6. (Color online) PSPS of pristine and biased β_{12}-borophene for two (a) homogeneous and (b) inversion symmetric models versus temperature.

a and b atoms, while the second one is comprised of d and e atoms. These sublattices are biased as $V = \{+V, +V, 0, -V, -V\}$ due to the above-mentioned symmetries and isotropies. Of course, we could model it in another way in our future researches. Consequently,

$$\hat{\mathcal{H}}^{\mathrm{EF}}_{\vec{k}} = \begin{pmatrix} \varepsilon_a + V & t_{ab}g_{\vec{k}} & t_{ac}f^*_{\vec{k}} & 0 & t_{ae}f_{\vec{k}} \\ t_{ab}g^*_{\vec{k}} & \varepsilon_b + V & t_{bc}g_{\vec{k}} & t_{bd}f^*_{\vec{k}} & 0 \\ t_{ac}f_{\vec{k}} & t_{bc}g^*_{\vec{k}} & \varepsilon_c & t_{cd}g_{\vec{k}} & t_{ce}f^*_{\vec{k}} \\ 0 & t_{bd}f_{\vec{k}} & t_c g^*_{\vec{k}} & \varepsilon_d - V & t_{de}g_{\vec{k}} \\ t_{ae}f^*_{\vec{k}} & 0 & t_{ce}f_{\vec{k}} & t_{de}g^*_{\vec{k}} & \varepsilon_e - V \end{pmatrix}, \tag{20}$$

Thus, PSPS of biased β_{12}-borophene can be calculated in terms of DOS which can be calculated using $\mathcal{D}(\mathcal{E}) = -(1/\pi N_a)\sum_{\vec{k}\in FBZ}\sum_{\alpha=1}^{5} \mathrm{Im}\left[1/(\mathcal{E}+\mathrm{i}\eta)\hat{\mathbf{I}} - \hat{\mathcal{H}}^{\mathrm{EF}}_{\vec{k}}\right]$.

In Fig. 6, for the unbiased and biased β_{12}-borophene in the case of (a) homogeneous and (b) inversion symmetric model, the PSPS versus temperature is shown. As it is explained from Ref. [26], the van Hove singularities in the electronic DOS are altered when the electric field changes the system dynamics. As a result of this, the PSPS is affected. Since the electronic phase transition emerges at high enough bias potentials, we expect a higher PSPS at stronger bias voltages. This can be observed in both models. From this expectation, one can see that in Fig. 6(a), the height of χ and T_N of the homogeneous models reduce as the applied perpendicular electric field is increased. On the other hand, for the most relevant experimental model, i.e. inversion symmetric model shown in panel (b), it is clear that applying an electric field leads to a decrease in the height of χ and the maximum point. As it is shown in the figure, a reduction of the Neel temperature in the inversion symmetric model is more smooth compared to the homogeneous one. This is another confirmation for the invalidity of the homogeneous model. We can observe that in both models, by increasing the strength of applied bias voltage the value of PSPS increases first at fairly low temperatures, while it increases in the intermediate temperatures, leading to a decrease in the susceptibility compared to unbiased β_{12}-borophene. At high enough temperatures, the PSPS decreases slightly with the bias voltage and it is expected to converge at the end.

5. Conclusions

To summarize, we have investigated the influence of dilute charged impurity and perpendicular electric field on the temperature-dependent Pauli spin paramagnetic susceptibility of β_{12}-borophene. In doing so, the five-band Hamiltonian homogeneous and inversion (non)symmetric models are implemented besides the Green's function technique. In the absence of the above-mentioned perturbations, the inversion symmetric model of the system dynamics shows an antiferromagnetic phase like graphene and the Dirac fermions are mostly play role in the response function. In the presence of a dilute charged impurity, the susceptibility fluctuates with the impurity concentration and scattering potential and there is no good order for the temperature trends, while in the presence of the electric field, it increases (decreases) slightly at low (intermediate and high) temperatures. From these results, we claim that the Neel temperature of β_{12}-borophene can be tuned with the applied electric field as well as the impurity concentration and scattering potential. The findings provide useful information for further researches and increase borophene applications in the logic electronic and spintronic devices.

Declaration of competing interest

The authors declare that they have no known competing financial interests or personal relationships that could have appeared to influence the work reported in this paper.

CRediT authorship contribution statement

Khang D. Pham: Investigation, Data curation, Formal analysis, Writing - Review & Editing. **Nguyen D. Hien:** Software, Formal analysis. **Nguyen N. Hieu:** Investigation, Formal analysis, Writing - review and editing, Conceptualization, Funding acquisition. **Le T.T. Phuong:** Conceptualization, Methodology, Investigation, Formal analysis, Writing - review and editing.

Acknowledgment

This research is funded by the Vietnam National Foundation for Science and Technology Development (NAFOSTED) under Grant No. 103.01-2017.309.

Appendix A. The relation between DOS and the green's functions

In order to find the DOS of a system, consider a system described by a Hamiltonian $\mathcal{H}$, being ψ_m and $\mathcal{E}_m$ its normalized eigenfunctions and eigenvalues (supposed to be countable, for simplicity). The total DOS of the system is defined as

$$D(\mathcal{E}) = \sum_m \delta(\mathcal{E} - \mathcal{E}_m), \tag{A.1}$$

By considering an arbitrary element ν with the orbital wave-function ϕ_ν we can write the Green's functions as

$$\begin{aligned} G_{\nu\nu}(E) =& \langle\phi_\nu| \frac{1}{\mathcal{E} + \mathrm{i}\eta - \hat{\mathcal{H}}} |\phi_\nu\rangle \\ =& \sum_m \langle\phi_\nu|\psi_m|\phi_\nu|\psi_m\rangle\langle\psi_m| \frac{1}{\mathcal{E} + \mathrm{i}\eta - \hat{\mathcal{H}}} |\phi_\nu\rangle \\ =& \sum_m \langle\phi_\nu|\psi_m|\phi_\nu|\psi_m\rangle\langle\phi_\nu| \frac{1}{\mathcal{E} - \mathrm{i}\eta - \hat{\mathcal{H}}} |\psi_m\rangle^\star \\ =& \sum_m |\langle\phi_\nu|\psi_m|\phi_\nu|\psi_m\rangle|^2 \left(\frac{1}{\mathcal{E} - \mathcal{E}_m + \mathrm{i}\eta}\right) \end{aligned} \tag{A.2}$$

or equivalently,

$$\begin{aligned} G_{\nu\nu}(E) =& \langle\phi_\nu| \frac{1}{\mathcal{E} + \mathrm{i}\eta - \hat{\mathcal{H}}} |\phi_\nu\rangle \\ =& \sum_m |\langle\phi_\nu|\psi_m|\phi_\nu|\psi_m\rangle|^2 \left(\frac{\mathcal{E} - \mathcal{E}_m - \mathrm{i}\eta}{(\mathcal{E} - \mathcal{E}_m)^2 + \eta^2}\right). \end{aligned} \tag{A.3}$$

Considering its imaginary part and the following definition of the Dirac delta function:

$$\delta(x) = \lim_{a\to 0} \frac{1}{\pi} \frac{a}{a^2 + x^2}, \tag{A.4}$$

we can quickly deduce that

$$\lim_{\eta\to 0} \mathrm{Im}\, G_{\nu\nu}(E) = -\pi \sum_m |\langle\phi_\nu|\psi_m|\phi_\nu|\psi_m\rangle|^2 \delta(\mathcal{E} - \mathcal{E}_m), \tag{A.5}$$

Consequently the DOS can be expressed as

$$D(\mathcal{E}) = \sum_\nu D_\nu(\mathcal{E}) = -\frac{1}{\pi} \lim_{\eta\to 0} \sum_\nu \mathrm{Im}\, G_{\nu\nu}(\mathcal{E}). \tag{A.6}$$

Appendix B. The relation between DOS and PSPS

To obtain the PSPS relation, one needs the condition that the external magnetic field is weak enough, which can be derived as follows:

$$\mathcal{M} = \frac{\mu_\mathrm{B}}{2} \int_0^\infty D(\mathcal{E}) d\mathcal{E} \left[f(\mathcal{E} - \mu_\mathrm{B}\mathcal{B}) - f(\mathcal{E} + \mu_\mathrm{B}\mathcal{B}) \right], \tag{B.1}$$

To carry out the integral, we expand the Fermi–Dirac distribution functions as

$$f(\mathcal{E} \pm \mu_\mathrm{B}\mathcal{B}) = f(\mathcal{E}) \pm \mu_\mathrm{B}\mathcal{B} \left(\frac{\partial f(\mathcal{E}, T)}{\partial \mathcal{E}}\right) + \cdots, \tag{B.2}$$

For weak magnetic fields $\mathcal{B} \to 0$ we can ignore the terms including higher orders of magnetic field $\mathcal{B}$, deducing

$$\begin{aligned} \mathcal{M} =& \frac{\mu_\mathrm{B}}{2} \int_0^\infty D(\mathcal{E}) d\mathcal{E} \left[f(\mathcal{E}) - \mu_\mathrm{B}\mathcal{B} \frac{\partial f(\mathcal{E}, T)}{\partial \mathcal{E}} \right. \\ & \left. - \left(f(\mathcal{E}) + \mu_\mathrm{B}\mathcal{B} \frac{\partial f(\mathcal{E}, T)}{\partial \mathcal{E}} \right) \right], \end{aligned} \tag{B.3}$$

So, we have

$$\mathcal{M} = \mu_\mathrm{B}^2 \mathcal{B} \int_0^\infty D(\mathcal{E}) \frac{-\partial f(\mathcal{E}, T)}{\partial \mathcal{E}} d\mathcal{E}, \tag{B.4}$$

References

[1] A.J. Mannix, X.F. Zhou, B. Kiraly, J.D. Wood, D. Alducin, B.D. Myers, X. Liu, B.L. Fisher, U. Santiago, J.R. Guest, M.J. Yacaman, A. Ponce, A.R. Oganov, M.C. Hersam, N.P. Guisinger, Science 350 (2015) 1513.
[2] B. Feng, J. Zhang, Q. Zhong, W. Li, S. Li, H. Li, P. Cheng, S. Meng, L. Chen, K. Wu, Nature Chem. 8 (2016) 563.
[3] E.S. Penev, A. Kutana, B.I. Yakobson, Nano Lett. 16 (2016) 2522.
[4] S.G. Xu, Y.J. Zhao, J.H. Liao, X.B. Yang, H. Xu, Nano Res. 9 (9) (2016) 2616.
[5] A. Lopez-Bezanilla, P.B. Littlewood, Phys. Rev. B 93 (2016) 241405(R).
[6] J. Carrete, W. Li, L. Lindsay, D.A. Broido, L.J. Gallego, N. Mingo, Mater. Res. Lett. 1 (2016) 204.
[7] C. Kamal, A. Chakrabarti, M. Ezawa, New J. Phys. 17 (2015) 083014.
[8] T. Ogitsu, E. Schwegler, G. Galli, Chem. Rev. 113 (5) (2013) 3425.
[9] X. Wu, J. Dai, Y. Zhao, Z. Zhuo, J. Yang, X.C. Zeng, ACS Nano 6 (8) (2012) 7443.
[10] D. Ciuparu, R.F. Klie, Y. Zhu, L. Pfefferle, J. Phys. Chem. B 108 (13) (2004) 3967.
[11] E.S. Penev, S. Bhowmick, A. Sadrzadeh, B.I. Yakobson, Nano Lett. 12 (5) (2012) 2441.
[12] H.J. Zhai, Y.F. Zhao, W.L. Li, Q. Chen, H. Bai, H.S. Hu, Z.A. Piazza, W.J. Tian, H.G. Lu, Y.B. Wu, Y.W. Mu, G.F. Wei, Z.P. Liu, J. Li, S.D. Li, L.S. Wang, Nature Chem. 6 (8) (2014) 727.
[13] H. Wang, Q. Li, Y. Gao, F. Miao, X.F. Zhou, X.G. Wan, New J. Phys. 18 (2016) 073016.
[14] F. Meng, X. Chen, S. Sun, J. He, Physica E 91 (2017) 106.
[15] M. Yarmohammadi, Phys. Lett. A 380 (48) (2016) 4062.
[16] M. Yarmohammadi, J. Electron. Mater. 45 (10) (2016) 4958.
[17] Y. Liu, Y.-J. Dong, Z. Tang, X.-F. Wang, Lu Wang, T. Hou, H. Lin, Y. Li, J. Mater. Chem. C 4 (2016) 6380.
[18] X. Yang, Y. Ding, J. Ni, Phys. Rev. B 77 (2008) 041402(R).
[19] J. Yuan, L.W. Zhang, K.M. Liew, RSC Adv. 5 (2015) 74399.
[20] H. Liu, J. Gao, J. Zhao, Sci. Rep. 3 (2013) 3238.
[21] J.Y. Li, H.Y. Lv, W. Lu, D.F. Shao, R.C. Xiao, Y.P. Sun, Phys. Lett. A 380 (46) (2016) 3928.

[22] L. Adamska, S. Sharifzadeh, ACS Omega 2 (2017) 8290.
[23] X. Zhang, J. Hu, Y. Cheng, H.Y. Yang, Y. Yao, S.A. Yang, Nanoscale 8 (33) (2016) 15340.
[24] B. Peng, H. Zhang, H. Shao, Yuanfeng Xu, R. Zhang, H. Zhu, J. Mater. Chem. C 4 (2016) 3592.
[25] B. Peng, et al., Mater. Res. Lett. 5 (6) (2017) 399.
[26] P.T.T. Le, T.C. Phong, M. Yarmohammadi, Phys. Chem. Chem. Phys. 21 (2019) 21790.
[27] M. Ezawa, Phys. Rev. B 96 (2017) 035425.
[28] M. Yarmohammadi, M. Zareyan, Chin. Phys. B 25 (6) (2016) 068105.
[29] B.D. Hoi, M. Yarmohammadi, Phys. Lett. A 382 (2018) 3298.
[30] M. Yarmohammadi, Phys. Rev. B 98 (15) (2018) 155424.
[31] B. Feng, O. Sugino, R.-Y. Liu, J. Zhang, R. Yukawa, M. Kawamura, T. Iimori, H. Kim, Y. Hasegawa, H. Li, et al., Phys. Rev. Lett. 118 (2017) 09640.
[32] V. Shukla, A. Grigoriev, N.K. Jena, R. Ahuja, Phys. Chem. Chem. Phys. 20 (2018) 22952.
[33] N.W. Ashcroft, N.D. Mermin, Solid State Physics, Thomson, Brooks/Cole, Singapore, 2006.
[34] W. Nolthing, A. Ramakanth, Quantum Theory of Magnetism, Springer, New York, 2009.
[35] M. Yarmohammadi, Solid State Commun. 250 (2017) 84.
[36] M. Yarmohammadi, Phys. Lett. A 381 (14) (2017) 1261.
[37] P.T.T. Le, M. Davoudiniya, M. Yarmohammadi, J. Appl. Phys. 125 (21) (2019) 213903.
[38] B.D. Hoi, M. Yarmohammadi, M. Davoudiniya, Solid State Commun. 271 (2018) 21.
[39] G.D. Mahan, Many Particle Physics, Plenum Press, NewYork, 1993.
[40] A.A. Avetisyan, B. Partoens, F.M. Peeters, Phys. Rev. B 79 (2009) 035421.
[41] J.E. Padilha, R.B. Pontes, A. Fazzio, J. Phys.: Condens. Matter 24 (2012) 075301.
[42] S. Yuan, E. van Veen, M.I. Katsnelson, R. Roldan, Phys. Rev. B 93 (2016) 245433.